Journal of Catalysis 278 (2011) 329–335

Contents lists available at ScienceDirect

Journal of Catalysis

journal homepage: www.elsevier.com/locate/jcat

Enhancing hydrogen production activity and suppressing CO formation from photocatalytic biomass reforming on Pt/TiO_2 by optimizing anatase–rutile phase structure

Qian Xu [a,b], Yi Ma [a,b], Jing Zhang [a], Xiuli Wang [a,b], Zhaochi Feng [a], Can Li [a,*]

[a] State Key Laboratory of Catalysis, Dalian Institute of Chemical Physics, Chinese Academy of Sciences, 457 Zhongshan Road, Dalian 116023, China
[b] Graduate University of Chinese Academy of Sciences, Beijing 100049, China

ARTICLE INFO

Article history:
Received 4 May 2010
Revised 22 December 2010
Accepted 4 January 2011

Keywords:
Hydrogen production
Ultra-low CO
Photocatalytic biomass reforming
Anatase–rutile phase structure
Photocatalyst

ABSTRACT

The photocatalytic activity in hydrogen production from biomass reforming can be significantly enhanced while keeping ultra-low CO concentration in produced H_2 by tuning the anatase–rutile phase structures of Pt/TiO_2 photocatalysts. Compared with Pt/P25, the overall photocatalytic activity for the photocatalyst with optimized anatase–rutile structure can be enhanced up to 3–5 times, and the CO concentration in hydrogen can be reduced from several thousands ppm to 5 ppm. It is proposed that the anatase–rutile phase structure can not only enhance the charge separation, consequently the activity, but also adjust the surface acid/base property which suppresses the CO formation.

1. Introduction

The depleting of fossil fuel reserves and the increasing environmental pollution promote the exploitation of clean and renewable energy. As a consequence of this situation, the interest in hydrogen has significantly increased in recent years. At present, almost 90% of hydrogen is produced from fossil fuels. Therefore, the development of technologies for hydrogen production from renewable energy sources is a fundamental way to deal with energy crisis and environmental problem.

Among the various technologies, hydrogen production via biomass reforming is one of the ideal solutions to deal with energy crisis and environmental problem [1–17]. The drawback of conventionally catalytic reforming biomass for hydrogen production is related to the harsh reaction conditions, such as complex process and the need for high temperature/pressure, resulting in high energy consumption and low net energy output. In addition, the complexity of by-products brings difficulties in separation and purification. More fatally, CO concentration in primary hydrogen is relatively high, usually more than 1%. Accordingly, an effective route of reforming biomass for hydrogen production with ultra-low CO concentration is cried for, in terms of long-term development.

The photocatalytic hydrogen production from biomass reforming under mild conditions has been attracting considerable attention [9–17] due to its potential industrial applications. Most of the studies on photocatalytic biomass reforming have focused on TiO_2-based photocatalysts [18–23]. Degussa P25, a commercial TiO_2, composed of approximately 80% anatase and 20% rutile [24,25], is considered as a benchmark model catalyst for its high photocatalytic reactivity, which is ascribed to the synergistic effect between anatase and rutile. However, the microstructure of P25 [26,27] and the essential reason for the excellent performance of P25 in photocatalysis are not well understood and still on controversy. The knowledge of the structure is of great importance in understanding the intrinsic factors contributing to the enhanced photocatalytic activity of P25 with anatase–rutile mixed phases. We have addressed previously that the formation of surface-phase junctions can make a significant enhancement in the photocatalytic activity of TiO_2 photocatalyst for hydrogen production [28]. This finding implies that the photocatalytic performance of TiO_2 could be further improved by elaborately designing the anatase–rutile structure.

Herein, we report our recent progress on hydrogen production in photocatalytic biomass reforming using thermal-treated P25 photocatalysts with tuned anatase–rutile structure. Surprisingly, we found that the photocatalytic activity for hydrogen production can be greatly increased, and furthermore, the CO concentration in H_2 can be reduced to an ultra-low level. Compared with P25 without any treatment, the overall photocatalytic activity for hydrogen

* Corresponding author. Fax: +86 411 84694447.
E-mail address: canli@dicp.ac.cn (C. Li).
URL: http://www.canli.dicp.ac.cn (C. Li).

0021-9517/$ - see front matter © 2011 Elsevier Inc. All rights reserved.
doi:10.1016/j.jcat.2011.01.001

production on thermal-treated P25 can be enhanced up to 3–5 times, and the CO concentration in hydrogen can be reduced at least by two orders of magnitude, namely from several thousands ppm to less than 5 ppm. It is proposed that the anatase–rutile junction structure is mainly responsible for the improved photocatalytic performance.

2. Experimental

2.1. Materials

P25 used in this work was obtained from Degussa (rutile fraction is about 12% as estimated from the integrated intensities of rutile (1 1 0) and anatase (1 0 1) diffractions in XRD [29]). Thermal-treated P25 photocatalysts (denoted as P25-*x*%R, where *x* indicates the rutile content estimated by XRD. For P25-100%R-a, b, c, d photocatalysts, where a, b, c and d indicate different treatment conditions) with different crystal phase structures were prepared by subtly tuning calcination temperature and calcination time.

All of the chemical reagents used in the experiments were of analytical grade: P25 (Degussa Co.); methanol, propanetriol, formic acid (Kermel Co.); glucose (Shenyang chemical reagent factory); $H_2PtCl_6{\cdot}6H_2O$ (Sinopharm Chemical Reagent Co.).

2.2. Characterization

UV Raman spectra were recorded at room temperature with a Jobin–Yvon T64000 triple-stage spectrograph with spectral resolution of 2 cm^{-1}. The photoluminescence spectra were measured on home-built laser-induced luminescence spectrograph, and the signal was collected with an ellipsoidal collecting mirror and focused onto a 320-mm monochromator. A 325-nm He–Cd laser was used as an exciting source for the measurement of UV Raman and photoluminescence spectra. Visible Raman spectra were recorded at room temperature on home-built Raman spectrograph with the excitation line at 532 nm. X-ray powder diffraction (XRD) patterns were recorded from 20–80° at a speed of 5°/min on a Rigaku D/Max-2500/PC powder diffraction system using Cu Kα radiation (40 kV and 100 mA). Transmission electron microscopy (TEM) was performed using a JEOL JEM-2000EX and a FEI Tecnai G^2 Spirit at an acceleration voltage of 120 kV. HRTEM images were obtained on Tecnai G^2 F30 S-Twin (FEI company). The pyridine adsorption infrared spectra were measured with a resolution of 4 cm^{-1} using 32 scans on a Fourier transform infrared spectrometer (Nicolet NEXUS 470) with a DTGS detector. The experiments were carried out in a special IR cell in conjunction with a water-cooling system and a vacuum system. There are several steps in the experimental procedure. The sample, typically 20 mg of titania, was first pressed into a self-supporting thin wafer (15 mm diameter) and then it was moved into the sample holder in the special IR cell. The wafer was evacuated from a vacuum system for 1 h to remove any impurities in the cell, and then the background spectrum of the sample was recorded. After the equilibration of the adsorbed pyridine vapor for 15 min, the wafer was degassed under vacuum conditions at 423 K for 30 min before the spectrum was recorded.

2.3. Photocatalytic reaction

Photocatalytic reaction was performed in a top-irradiation-type Pyrex reaction cell connected to a closed gas circulation and evacuation system under 300-W Xe lamp. A shutter window filled with water was placed between the Xe lamp and the reaction cell to remove infrared light illumination. Prior to illumination, the reactor is deaerated by evacuation. The whole system includes reaction system, sample chamber and analysis system. It should be mentioned that the three parts are separated by valves. The sample chamber is continuous with the reaction system by opening the three-way valve. After sampling completed, the three-way valve is closed and the evolved gas is analyzed online by gas chromatography, which is equipped with a thermal conductivity detector, a flame-ionization detector and a methanizer. The amount of hydrogen is measured by the thermal conductivity detector. The flame-ionization detector is used to analyze CO and CO_2, which are converted into CH_4 after passing the methanizer. Once the gas analysis completed, the four-way valve between the sample chamber and analysis system is closed and the sample chamber is deaerated by evacuation. In our experiments, the sampling and online analysis was performed per hour. Typically, photocatalyst (0.2 g) was suspended in 200 mL of aqueous solution ($C_{methanol}$ = 20 vol.%, $C_{propanetriol}$ = 20 vol.%, $C_{formic\ acid}$ = 20 - vol.%, $C_{glucose}$ = 1.3 mmol/L). Cocatalyst 0.1 wt.% Pt was loaded on TiO_2 by in situ photodeposition from precursor $H_2PtCl_6{\cdot}6H_2O$ under irradiation.

In situ photodeposition method: The $H_2PtCl_6{\cdot}6H_2O$ solution was added into the 200 mL aqueous solution containing TiO_2 photocatalyst and biomass model compound under vigorous stir. After the reaction system deaerated by evacuation, the reaction cell was illuminated by the Xe lamp from the top. The precursor H_2PtCl_6 was reduced by the excited elections on TiO_2 to metallic Pt at the very beginning of the reaction.

3. Results and discussion

The anatase–rutile structure was tuned by changing the calcination temperature. As presented in Fig. 1a, the diffraction patterns of anatase phase gradually diminish in intensity with the increase in the calcination temperature from 500 to 800 °C for 3 h, suggesting that the phase transformation from anatase to the rutile progressively proceeds at the elevated temperatures. The rutile contents estimated from the integrated intensities of rutile and anatase diffraction patterns in Fig. 1a were shown in Fig. 1b. It is obvious that the anatase gradually transforms into rutile; especially after P25 calcined at 700 °C for 3 h, the rutile content increases distinctly.

Photocatalytic reactions were carried out using methanol, propanetriol and glucose as model compounds of biomass. Fig. 2a shows the hydrogen production on thermal-treated P25 photocatalysts with different anatase–rutile structures. The photocatalytic activity of hydrogen production on P25 without treatment is included for comparison. The rates of H_2 production on P25 are about 475, 1492 and 2308 μmol g^{-1} h^{-1} for photocatalytic reforming of glucose, methanol and propanetriol, respectively. However, the photocatalytic activity of hydrogen production on Pt/P25-*x*%R photocatalysts can be greatly enhanced and reaches 749, 7094 and 7784 μmol g^{-1} h^{-1} on Pt/P25-74%R photocatalyst from the photocatalytic reforming of glucose, methanol and propanetriol, respectively. The photocatalytic activity of Pt/P25-100%R sample is lower than that of Pt/P25-74%R, but it is still much higher compared to that of Pt/P25.

It is noteworthy that the photocatalytic activity of hydrogen production from biomass reforming on Pt/P25-*x*%R outperforms that on the well-known photocatalyst Pt/P25. The photocatalytic performance is actually influenced by factors like crystallinity, crystalline structure, surface area, density of OH groups, surface acidity, and so on. Generally, the improvement of crystallization degree plays an important role in the enhancement of photocatalytic activity for thermal-treated photocatalysts. Thus, P25 was deliberately treated for a longer period of time and/or at higher temperature for the comparison of the surface-specific activity, i.e., the relationship between the amount of H_2 production and the surface area (μmol h^{-1} m^{-2}, shown in Fig. 2b). Compared with Fig. 2a and b suggests that the H_2 production against phase content agrees with the rates normalized for differences in surface area.

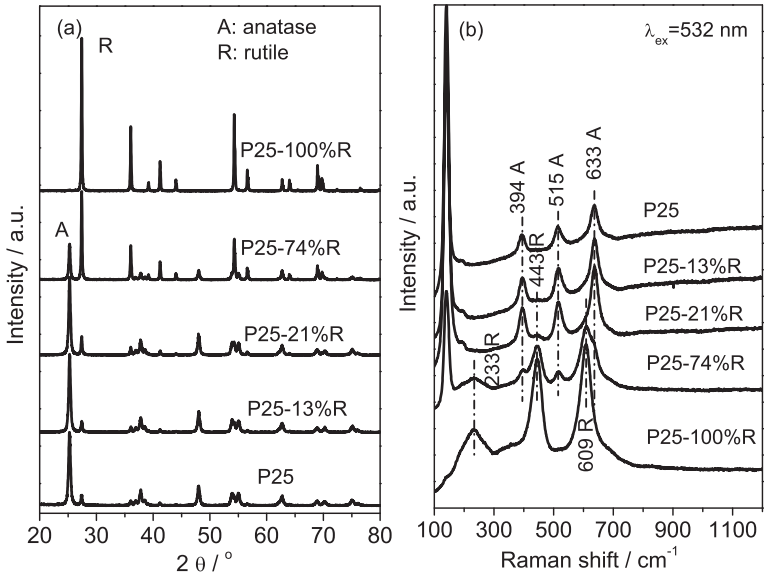

Fig. 1. (a) XRD patterns and (b) visible Raman spectra with the excitation lines at 532 nm of P25-*x*%R photocatalysts (where *x* indicates the rutile content estimated by XRD).

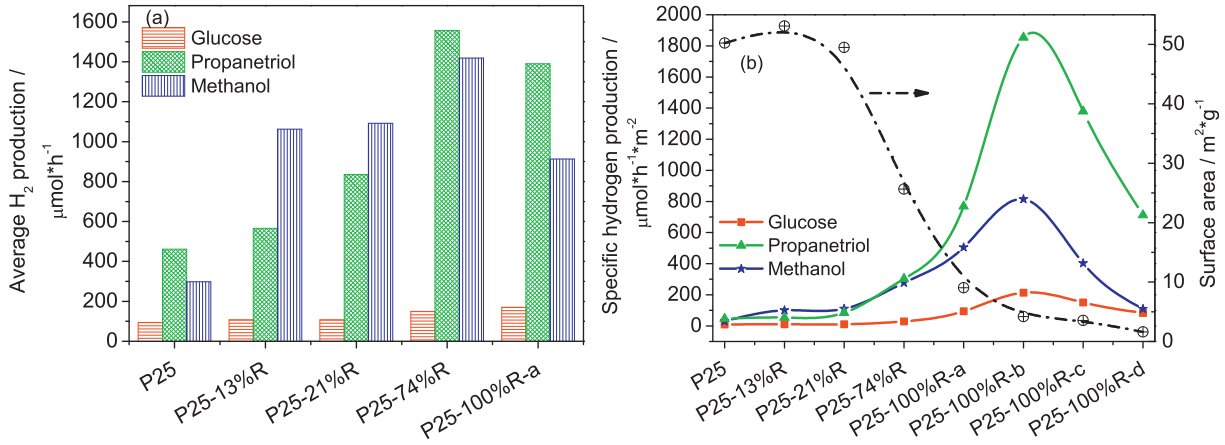

Fig. 2. (a) Average hydrogen production in photocatalytic reforming methanol, propanetriol and glucose and (b) surface-specific photocatalytic activity for hydrogen production in photocatalytic reforming methanol on Pt/P25-*x*%R photocatalysts (where *x* indicates the rutile content estimated by XRD. For P25-100%R-a, b, c, d photocatalysts, where a, b, c and d indicate different treatment conditions), the surface areas of P25-*x*%R photocatalysts are also displayed (dash dot).

Though the specific hydrogen production of P25-100%R-a (P25 calcined at 800 °C for 3 h) is slightly higher than that of P25-74%R, the enhancement should be directly related to the decrease in surface area. P25-100%R-b (P25 calcined at 800 °C for 12 h) sample exhibits its superior surface-specific photocatalytic activity for hydrogen production. The rates of hydrogen production on P25-100%R-c (P25 calcined at 850 °C for 12 h) and P25-100%R-d (P25 calcined at 900 °C for 12 h) decreases with the increase in the treatment temperature. Especially, it can be seen from Fig. 2b that the rate of hydrogen production on P25-100%R-d is far lower than that on P25-100%R-b, and even lower than that on P25.

In the calcination temperature ranging from 500 to 900 °C, the specific photocatalytic activity of thermal-treated P25 increases with increasing calcination temperature and reaches maximum at ca. 800 °C for 12 h. Further increase in the treatment temperature does not increase the photocatalytic activity. Instead, the photocatalytic activity decreases dramatically, even to the level of P25. Calcination at higher temperature favors the improvement in crystallinity. These results demonstrate that the crystallization degree is not the major responsibility for the super high photocatalytic activity of the thermal-treated P25 photocatalysts.

To explore the intrinsic factor contributing to the enhancement of photocatalytic activity, the microstructures and surface properties of TiO_2-based photocatalysts were investigated.

Fig. 3 displays TEM and HRTEM images of TiO_2-based photocatalysts. Most particles in P25 exhibit diameters in a range between 20 and 80 nm with particles contacting each other (Fig. 3a). Under the lower temperature thermal treatment, the phase transformation is accompanied by the agglomeration of TiO_2 particles and the rutile phase progressively develops into the whole conglomeration by coalescing the neighboring anatase particles (Fig. 3b and c), while the obvious change of shape and particle size is hardly observed. With the increase in thermal treatment temperature to/above 700 °C, the particle size grows as large as 200 nm (Fig. 3d and e), especially TEM images (Fig. 3d) of P25-74%R show that the small particles (30–90 nm) are highly dispersed on the relatively large particles (~200 nm) with intimate contact. HRTEM (Fig. 3f) studies further provide crucial information on the spatial distribution of the phases. As shown in Fig. 3f, the small particles and larger particles show the atomic planes with a lattice spacing of 3.503 and 3.225 Å, respectively, which can be indexed into (1 0 1) atomic plane of anatase and (1 1 0) atomic plane of rutile,

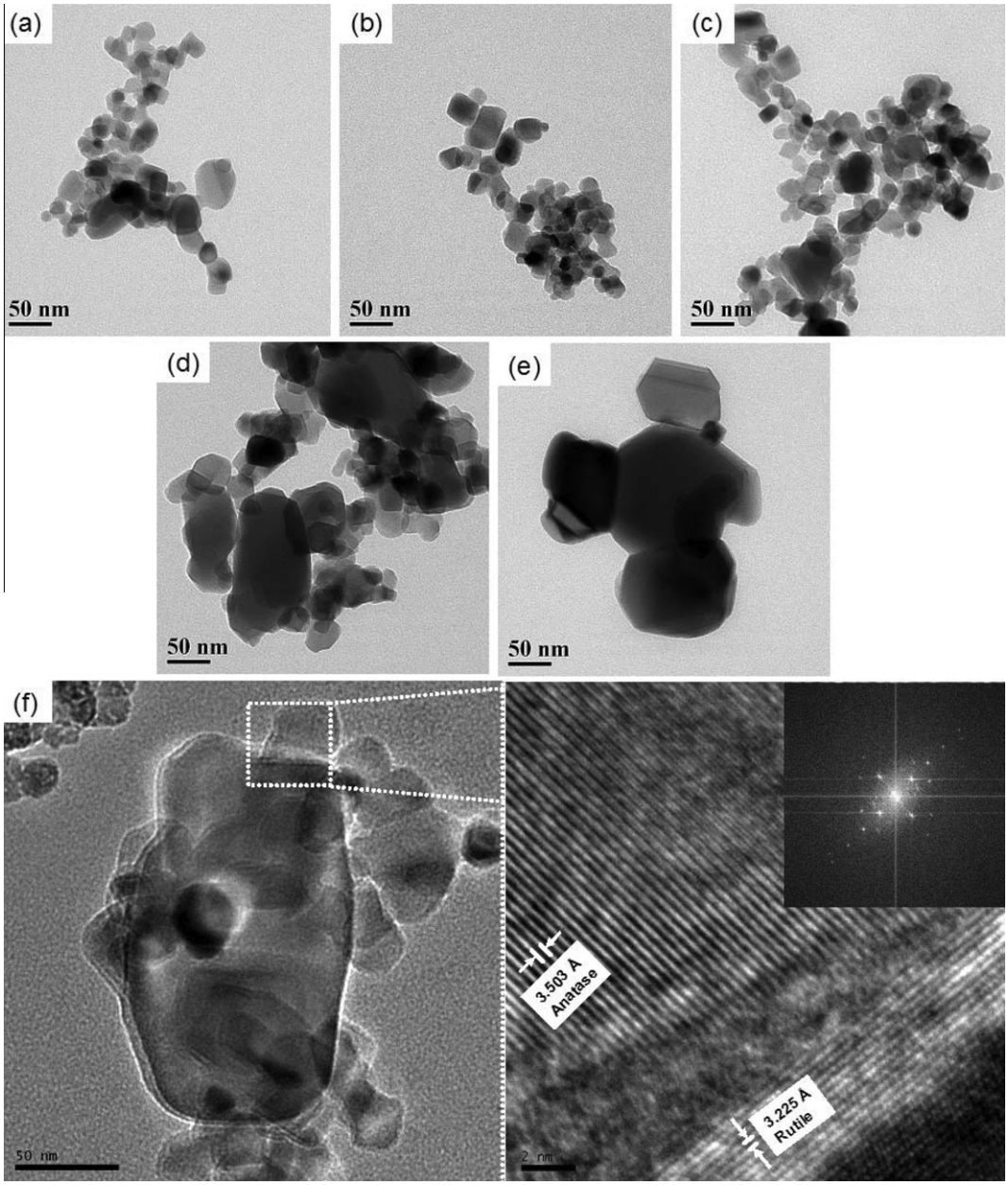

Fig. 3. TEM images of (a) P25, (b) P25-13%R, (c) P25-21%R, (d) P25-74%R, (e) P25-100%R-a and (f) HRTEM images of P25-74%R.

respectively. In addition, HRTEM displays the combination of surface anatase in intimate contact with rutile. HRTEM images together with TEM images provided direct evidence for the phase junction between anatase and rutile phase.

Fig. 4a shows the surface luminescence properties of TiO_2 photocatalysts. P25 displays a visible luminescence band centered at 495 nm. For P25 calcined at 500 and 600 °C for 3 h (noted as P25-13%R and P25-21%R), the luminescence bands are till located at 495 nm. By increasing the temperature to 700 °C, a near-infrared luminescence band centered at 835 nm appears. Upon further increasing the thermal treatment temperature above 700 °C, the band at 495 nm was quenched. The bands at 495 nm and 835 nm are associated with the surface oxygen vacancies of anatase phase and the intrinsic defects of rutile phase, respectively [30]. Considering XRD and visible Raman spectra (Fig. 1) of P25-100%R, no anatase phase is observed, it can be concluded that quenching of the band at 495 nm is actually due to the absence of the anatase phase. Furthermore, UV Raman spectra (Fig. 4b) indicate that the mixed phase of both anatase and rutile coexist in the surface region of P25-74%R, whereas the other samples are in either anatase or rutile phases. These results confirm that the surface-phase junction between anatase and rutile was formed in P25-74%R.

The adlineation at anatase–rutile interface facilitates photoinduced charge transfer across grain boundaries by spatially trapping electron and hole in different crystalline phases. Li et al. [31] contended that adlineation at solid–solid interfaces is one of the most important factors for effective interfacial charge transfer and improved photocatalytic activity. The more the amount of anatase–rutile junctions, the higher photocatalytic activity for hydrogen production is, as revealed in Fig. 2. There may be only trace amount of anatase phase remained in P25-100%R, which cannot be sensitively identified, and the relatively low photocatalytic activity might be related to the decrease in anatase–rutile junction concentration. The in situ NEXAFS studies [32] indicate that the anatase/rutile

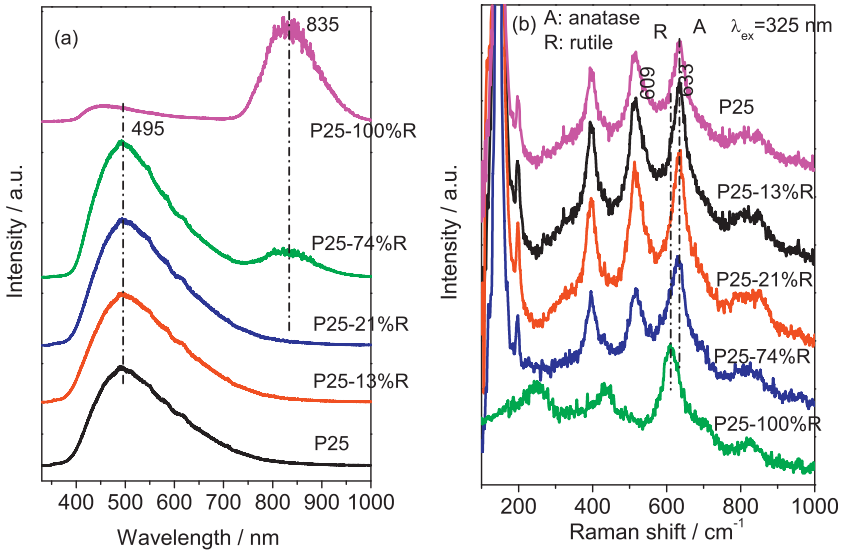

Fig. 4. (a) Photoluminescence spectra and (b) UV Raman spectra of P25-*x*%R photocatalysts (where *x* indicates the rutile content estimated by XRD).

phase boundary suppresses the hole-electron recombination, leading to improved photoreactivity of TiO_2. Thus, the spatial separation of photogenerated charge carriers explains the enhancement of the photocatalytic performance in biomass reforming. This effect is actually attributed to the differentiation in the relative energies of the two phases resulting in the possible formation of type II-like heterojunction, which can promote the photogenerated electron–hole separation [33,34]. Theoretical study has proved that the wavefunction for photogenerated electrons and holes will stay in the different region in type II heterojunction structure [35]. The photogenerated carriers may also greatly improve transport mobility at the interface between two oxide structures as reported previously, which could be the essential reason for the enhanced photocatalytic activity [36,37]. Crystallographically, three structure types are present [27] in P25: anatase, rutile and amorphous, which often exist in discrete units with close proximity. The high photocatalytic activity of Degussa P25 should originate from an unusual microstructure consisting of the anatase particles in contact with the rutile particles, creating interface across which photoinduced charge separation occurs. Under thermal treatment, crystallites are gradually transformed from amorphous to crystalline phase accompanied by the anatase–rutile phase transformation, owing to thermostimulated removal of hydroxyl group at higher calcination temperature. Then, the amount of anatase–rutile interfacial sites served as the active centers for charge separation increase, and consequently, the photocatalytic activity is significantly enhanced. Therefore, the anatase–rutile phase junction with considerable concentration is a crucial factor for the enhancement of the photocatalytic activity of the thermal-treated P25.

Using Pt/P25 as a photocatalyst, we found that the CO concentration in hydrogen (expressed as the molar ratio of CO/H_2) produced by photocatalytic reforming of glucose, methanol and propanetriol was 54,691, 6387 and 6649 ppm, respectively (Fig. 5a). This limits the application of the produced hydrogen directly to the fuel cell due to the CO poisoning of the noble metal catalyst in the fuel cell. However, decrease in CO concentration in hydrogen to ultra-low level is quite difficult for the biomass reforming. Interestingly, for photocatalytic reforming reaction on thermal-treated P25 photocatalysts, the CO concentration is dramatically decreased. For example, in Pt/P25-*x*%R, it is decreased from 54,691, 6387 and 6649 ppm to 6568, 34.8 and 76.3 ppm in photocatalytic reforming of glucose, methanol and propanetriol, respectively. Under an optimized experimental condition, the best of our TiO_2-based photocatalyst can reduce the CO concentration even to less than 5 ppm, which merrily satisfies the ultra-low CO concentration requirements for the direct application of the hydrogen in the fuel cell technology.

The desired photocatalytic biomass reforming to produce hydrogen proceeds by the dehydrogenation of oxygenate species to produce CO_2, while this reaction is always accompanied by a dehydration reaction with the formation of by-product CO. Formic acid-like species is a common intermediate producing CO_2 and H_2 or CO and H_2O in the photocatalytic biomass reforming. In order to understand why the CO formation can be dramatically suppressed on the thermal-treated P25 photocatalysts, the photocatalytic performance of formic acid reforming on P25-*x*%R photocatalysts was investigated. As shown in Fig. 5b, the CO concentration in hydrogen (denoted as CO/H_2) and the proportion of CO to oxycarbide (denoted as CO/CO_2) decrease obviously after the thermal treatment to P25. The CO/CO_2 ratio toward dehydration or dehydrogenation of HCOOH is related to the acidity/basicity of the oxide surface [38], that is, basic oxide surfaces are in favor of the dehydrogenation pathway and the acidic surfaces tend toward the dehydration pathway. Thermal treatment to oxides induces the evolution of acidity/basicity owing to the removal of hydroxyl groups at the anatase–rutile interfacial sites during phase transformation from amorphous to crystalline phase and/or from anatase to rutile. Consequently, the acid strength is decreased, which is in favor of dehydrogenation reaction. In other words, the change of surface acidity/basicity at the interfacial site should be responsible for the suppression of CO in photocatalytic biomass reforming on thermal-treated P25.

Fig. 6 shows the FT-IR spectra of the pyridine adsorbed on P25-*x*%R photocatalysts. The IR bands at 1604 and 1445 cm^{-1} correspond to the coordinate pyridine adsorbed on Lewis acid sites and that at 1492 and 1575 cm^{-1} are assigned to Brønsted and Lewis acid site [39], while P25-*x*%R photocatalysts do not reveal the Brønsted acidity around 1540 cm^{-1}. It is obvious that the absorbed pyridine gradually decrease with increasing rutile content, suggesting the decrease in acidity, which further demonstrates that the suppression of CO should be correlated with the decrease in surface acidity.

The enhancement of hydrogen production and suppression of CO concentration on TiO_2-based photocatalysts with tuned

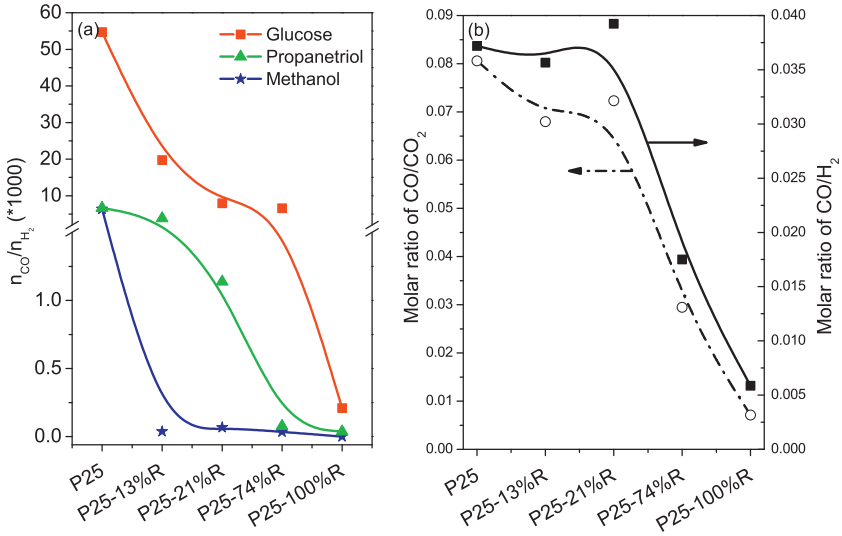

Fig. 5. (a) Molar ratio of CO/H_2 in photocatalytic reforming methanol, propanetriol and glucose, (b) molar ratio of CO/H_2 (square, solid) and CO/CO_2 (circle, open) in photocatalytic reforming formic acid on Pt/P25-*x*%R photocatalysts (where *x* indicates the rutile content).

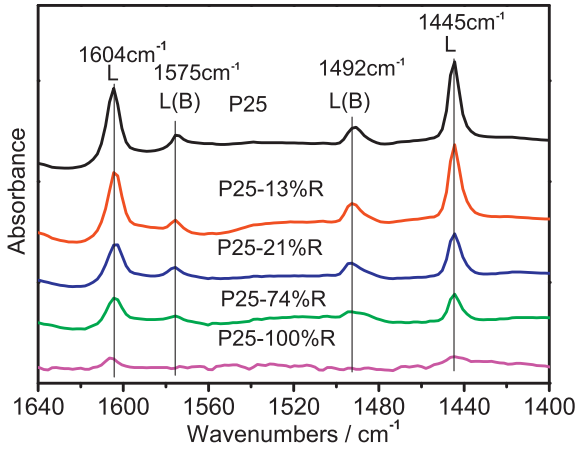

Fig. 6. FT-IR spectra of pyridine adsorbed on P25-*x*%R photocatalysts (where *x* indicates the rutile content). B: Brønsted acid sites; L: Lewis acid sites.

anatase–rutile structure was further observed in photocatalytic reforming methanol on P25 calcined at 700 °C for different time periods (denoted as P25-700-t, in which t indicates the calcination time). The photocatalytic activity of hydrogen production and CO concentration in produced hydrogen on Pt/P25-700-t are depicted in Fig. S2a and b (The corresponding XRD, the rutile content, visible Raman spectra and photoluminescence spectra are shown in Fig. S1). The hydrogen production was significantly enhanced by tuning the anatase–rutile structure, particularly in the formation of surface anatase–rutile junction. Meanwhile, the CO concentration in hydrogen was dramatically suppressed.

4. Conclusions

The photocatalytic performance of Pt/P25 photocatalyst for biomass reforming can be greatly enhanced by elaborately controlling the crystal phase structure of TiO_2. The anatase–rutile phase junction structure is beneficial for photoinduced charge separation and consequently the enhancement of photocatalytic activity. The by-product CO can be suppressed to an extremely low level, which can meet the requirements for the direct application in the fuel cell technology. Suppressing CO formation in photocatalytic biomass reforming is possibly attributed to the evolution of surface acidity/basicity at the interface of thermal-treated P25. The interfacial sites possibly favor the dehydrogenation of oxygenate species to produce CO_2. This work also helps us in understanding the excellent photocatalytic performance of P25.

Acknowledgments

This work was supported by the National Natural Science Foundation of China (NSFC, Grant No. 20673112), the National Basic Research Program of China (Grant No. 2009CB220010) and Solar Energy Project of Chinese Academy of Sciences (Grant No. KGCX2-YW-391-1). We also thank Dr. Hongxian Han for his help in revising this manuscript and discussion.

Appendix A. Supplementary material

Supplementary data associated with this article can be found, in the online version, at doi:10.1016/j.jcat.2011.01.001.

References

[1] R.C. Saxena, D.K. Adhikari, H.B. Goyal, Renew. Sust. Energy Rev. 13 (2009) 156.
[2] G.A. Deluga, J.R. Salge, L.D. Schmidt, X.E. Verykios, Science 303 (2004) 993.
[3] R.D. Cortright, R.R. Davda, J.A. Dumesic, Nature 418 (2002) 964.
[4] J. Llorca, P.R. de la Piscina, J. Sales, N. Homs, Chem. Commun. 641 (2001).
[5] A.N. Fatsikostas, D.I. Kondarides, X.E. Verykios, Chem. Commun. 851 (2001).
[6] A.N. Fatsikostas, D.I. Kondarides, X.E. Verykios, in: 3rd European Workshop on Environmental Catalysis, Maiori, Italy, 2001, p. 145.
[7] J.R. Rostrup-Nielsen, R. Nielsen, Catal. Rev. 46 (2004) 247.
[8] F. Joensen, J.R. Rostrup-Nielsen, J. Power Sour. 105 (2002) 195.
[9] M. Ni, M.K.H. Leung, D.Y.C. Leung, K. Sumathy, Renew. Sust. Energy Rev. 11 (2007) 401.
[10] T. Sakata, T. Kawai, Chem. Phys. Lett. 80 (1981) 341.
[11] M. Kawai, T. Kawai, S. Naito, K. Tamaru, Chem. Phys. Lett. 110 (1984) 58.
[12] T. Maruyama, T. Nishimoto, Ind. Eng. Chem. Res. 30 (1991) 1634.
[13] M. Ashokkumar, Int. J. Hydrogen Energy 23 (1998) 427.
[14] M.C. Blount, J.A. Buchholz, J.L. Falconer, J. Catal. 197 (2001) 303.
[15] G.R. Bamwenda, S. Tsubota, T. Nakamura, M. Haruta, J. Photochem. Photobiol. A 89 (1995) 177.
[16] Y.Q. Wu, G.X. Lu, S.B. Li, J. Photochem. Photobiol. A 181 (2006) 263.
[17] Y. Mizukoshi, Y. Makise, T. Shuto, J.W. Hu, A. Tominaga, S. Shironita, S. Tanabe, Ultrason. Sonochem. 14 (2007) 387.
[18] T. Kawai, T. Sakata, J. Chem. Soc. Chem. Commun. 694 (1980).
[19] Y.Z. Yang, C.H. Chang, H. Idriss, Appl. Catal. B – Environ. 67 (2006) 217.
[20] G.P. Wu, T. Chen, W.G. Su, G.H. Zhou, X. Zong, Z.B. Lei, C. Li, Int. J. Hydrogen Energy 33 (2008) 1243.

[21] G.P. Wu, T. Chen, X. Zong, H.J. Yan, G.J. Ma, X.L. Wang, Q. Xu, D.G. Wang, Z.B. Lei, C. Li, J. Catal. 253 (2008) 225.
[22] S. Fukumoto, M. Kitano, M. Takeuchi, M. Matsuoka, M. Anpo, Catal. Lett. 127 (2009) 39.
[23] X.B. Chen, S.S. Mao, Chem. Rev. 107 (2007) 2891.
[24] M. Janus, A.W. Morawski, Appl. Catal. B 75 (2007) 118.
[25] N. Bowering, G.S. Walker, P.G. Harrison, Appl. Catal. B – Environ. 62 (2006) 208.
[26] A.K. Datye, G. Riegel, J.R. Bolton, M. Huang, M.R. Prairie, J. Solid State Chem. 115 (1995) 236.
[27] R.I. Bickley, T. Gonzalezcarreno, J.S. Lees, L. Palmisano, R.J.D. Tilley, J. Solid State Chem. 92 (1991) 178.
[28] J. Zhang, Q. Xu, Z. Feng, M. Li, C. Li, Angew. Chem. Int. Ed. 47 (2008) 1766.
[29] A.A. Gribb, J.F. Banfield, Am. Miner. 82 (1997) 717.
[30] J.Y. Shi, J. Chen, Z.C. Feng, T. Chen, Y.X. Lian, X.L. Wang, C. Li, J. Phys. Chem. C 111 (2007) 693.
[31] G.H. Li, K.A. Gray, Chem. Phys. 339 (2007) 173.
[32] H. Jie, H. Park, K.H. Chae, M. Anpo, J.K. Park, Chem. Phys. Lett. 470 (2009) 269.
[33] B.Z. Tian, X.L. Zheng, T.J. Kempa, Y. Fang, N.F. Yu, G.H. Yu, J.L. Huang, C.M. Lieber, Nature 449 (2007) 885.
[34] J. Xiang, W. Lu, Y.J. Hu, Y. Wu, H. Yan, C.M. Lieber, Nature 441 (2006) 489.
[35] Y. Zhang, L.W. Wang, A. Mascarenhas, Nano Lett. 7 (2007) 1264.
[36] H.Y. Hwang, Science 313 (2006) 1895.
[37] A. Ohtomo, H.Y. Hwang, Nature 427 (2004) 423.
[38] M.A. Barteau, Chem. Rev. 96 (1996) 1413.
[39] M. Kobayashi, A. Morita, M. Ikeda, Appl. Catal. B 71 (2007) 94.